Potassium/Chloride Co-transporter 1 and 3 (KCC1/KCC3; SLC12A4/SLC12A6)

A Target Enabling Package (TEP)

Gene ID / UniProt ID / EC	6560/ Q9UP95
Target Nominator	Katharina L. Duerr
Authors	Gamma Chi[1], Rebecca Ebenhoch[1,6] , Henry Man[1,8], Haiping Tang[2], Laurence E. Tremblay[4], Gabriella Reggiano[3], Xingyu Qiu[2], Tina Bohstedt[1] , Patrizia Abrusci[1,8], Ben Tehan[7], Idlir Liko[7], Fernando Almeida[7], Alexandre P. Garneau[4,5], Dong Wang[1], Gavin McKinley[1], Shubhashish M.M. Mukhopadhyay[1], , Alejandra Fernandez-Cid[1], Samira Slimani[4], Julie L. Lavoie[5], Nicola Burgess-Brown[1], Frank DiMaio[3], Paul Isenring[4], Carol V. Robinson[2,7], and Katharina L. Düerr[1,7]
Target PI	Katharina L. Duerr (SGC Oxford)
Therapeutic Area(s)	Sickle cell disease (SCD), Neurological
Disease Relevance	Osmoregulation by KCC1 is involved in the sickling of red blood cells with patients suffering from sickle cell anaemia. Inactivating mutations of KCC3 are a direct cause of Andermann Syndrome, a neurological disorder disproportionately affecting French Canadian population.
Date Approved by TEP Evaluation Group	November 2020
Document version	Version 1.0
Document version date	November 2020
Citation	Gamma Chi, Rebecca Ebenhoch, Henry Man, Haiping Tang, Laurence E. Tremblay, Gabriella Reggiano, … Katharina L. Duerr. (2020). SLC12A4/SLC12A6; A Target Enabling Package [Data set]. Zenodo. http://doi.org/10.5281/zenodo.4436169
Affiliations	1 Structural Genomics Consortium, University of Oxford, Roosevelt Drive, Oxford, OX3 7DQ, UK 2 Physical and Theoretical Chemistry Laboratory, University of Oxford, South Parks Road, Oxford, OX1 3QZ, UK 3 Department of Biochemistry, University of Washington, 1705 NE Pacific St, Seattle, 98195, Washington, USA 4 Department of Medicine, Nephrology Research Group, Faculty of Medicine, Laval University, Quebec City, Québec, Canada 5 Cardiometabolic Axis, School of Kinesiology and Physical Activity Sciences, University of Montréal, Montréal, Quebec, Canada 6 Present address: MedChem, Boehringer Ingelheim Pharma GmbH & Co. KG, Birkendorferstrasse 65, 88397 Biberach, Germany 7 Omass Therapeutics, The Schrödinger Building, Heatley Road, Oxford Science Park, Oxford, OX4 4GE, UK 8 Present address: Exscientia, The Schrödinger Building, Heatley Road, Oxford Science Park, Oxford, OX4 4GE, UK

SUMMARY OF PROJECT

KCC1 (SLC12A4) and KCC3 (SLC12A6) are co-transporters of potassium and chloride, and members of cation-chloride co-transporter (CCC; or Solute Carrier 12) family. They regulate chloride level and cell volume via export of potassium

and chloride ions. KCC1 plays an important role in sickle cell diseases, where its activity leads to sickling of red blood cells, a key pathological feature of the disease. Hence, symptoms of this common genetic disorder can be significantly reduced by inactivation of KCC1. KCC3 is highly expressed in neurones, where its inherited defect can lead to a rare form of peripheral neuropathy, Andermann Syndrome. This TEP presents the structures of KCC1 and KCC3 in both wild-type and inactivated states, revealing structural mechanisms for their regulation. From these structures, we have identified ligands ATP and magnesium ion, and have subsequently used biophysical assay and mass spectrometry to characterise them. These can be exploited to develop small molecule modulators to treat sickle cell diseases, one of the most common genetic disorders with unmet needs, as well as neurological disorders.

SCIENTIFIC BACKGROUND

Potassium chloride co-transporters (KCCs) are a four-member branch of the CCC family, also known as SLC12s in the solute carrier transporter nomenclature (4). KCCs are primarily involved in the chloride homeostasis by exporting it across plasma membrane using potassium ion gradient generated by Na^+/K^+ ATPase, as well as cell volume regulation via K^+/Cl^--driven osmoregulation (**Fig 1**). KCC3 (SLC12A6) and KCC2 (SLC12A5) are highly expressed in the neuronal tissues (3,4), where they are involved in the maintenance of low chloride ion concentration in GABAergic neurons. This leads to activated gamma aminobutyric acid (GABA) and glycine receptors creating plasma membrane hyperpolarisation via influx of chloride ions. Conversely, inactivation of KCC3 and KCC2 raise chloride levels inside the cells, leading GABA receptors to depolarise the membrane instead via efflux of chloride ions.

Due to such important role of KCC3 in the neuronal response to neurotransmitters and cell volume homeostasis (3,4), its mutation can lead to debilitating neurological disorders. Various rare hereditary neurological diseases caused by loss-of-function mutations of KCC3 have been reported. The most significant of these is Andermann Syndrome (OMIM 218000), a form of peripheral neuropathy disproportionately affecting the French Canadian population (5,6). Gain-of-function mutation of KCC3 has also been reported to cause rare diseases, for example KCC3 p.T991A mutation causing motor neuropathy.

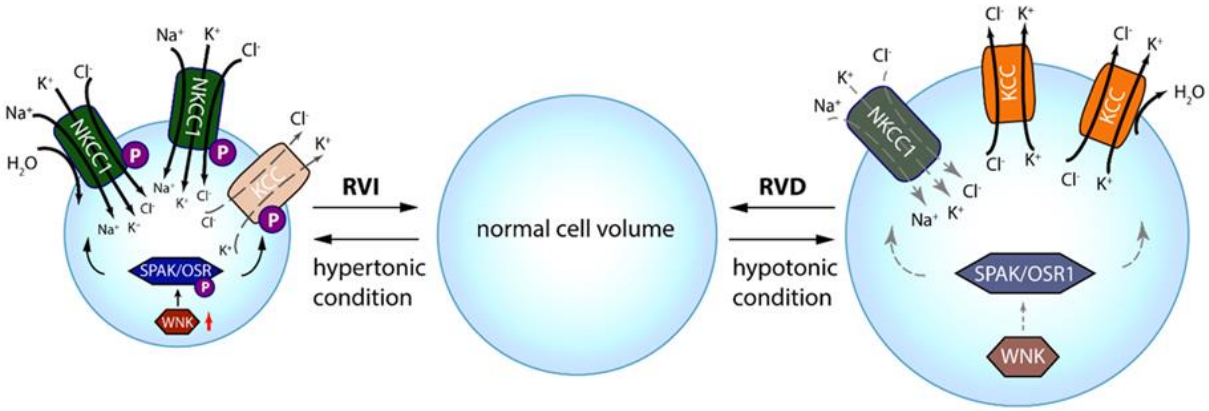

Figure 1. Schematic diagram of the regulation of NKCC1 and KCC transporters, courtesy of Huang, *et. al*. (3). Potassium and chloride ion export by KCC transporters is triggered under hypotonic conditions to lower intracellular osmolarity, which in turn restores normal cell volume by osmotic gradient.

KCC1 is highly expressed in red blood cells (7), where it has a secondary role in maintaining cell volume. KCC1 shows elevated expression in people with sickle cell genes (7,8), both carriers and symptomatic, the mechanism of which is not currently understood. Activation of KCC1 leads to dehydration of red blood cells, making them more vulnerable to haemoglobin polymerisation in patients with sickle cell genes. KCC1 is also part of the positive feedback loop of red blood cell sickling; haemoglobin polymerisation and eventual death of red blood cells lead to increased level of new red blood cells, which tend to have higher KCC1 activity than aged cells.

Due to this key role KCC1 plays in the pathogenesis of sickle cell diseases (SCD), its inactivating modulators hold significant potential for treating this disease. Inhibition of KCC1 activity can keep red blood cells hydrated in SCD patients (9), preventing them from undergoing cell sickling process. Several *in vivo* models confirm this: red blood cells were shown to remain hydrated and less prone to sickling in KCC-knockout mice, whereas its activating mutant would enhance SCD disease progression (10,11). Similar improvement in prognosis was observed for KCC1-knockout mice with β-thalassaemia (12), another genetic disease caused by defective haemoglobin. Therefore, specific inhibitors of KCC1 can be used for long-term treatment for SCD and β-thalassaemia, two of the most common genetic diseases and those with significant unmet needs.

Several pan-KCC inhibitors have been reported in the literature, however, those selective to specific members are yet to be found (13). Both [dihydroindenyl-oxy] alkanoic acid (DIOA) (14) and later-discovered synthetic compounds such as VU0463271 (15) have been shown to inhibit a broad range of KCC transporters (10,15-17), limiting their use as therapeutic agents. Developing compounds specific to each member will require structural information on its activation and regulation mechanism as well as potential binding pocket. This TEP aims to address these gaps.

RESULTS – THE TEP

Protein expression and purification

Various constructs of KCC1 and KCC3b (B isoform of KCC3) with Strep-II and 10-His tags were individually expressed in Human Embryonic Kidney (HEK293) cell line. KCC1/KCC3b were extracted from cell membrane by solubilisation with lauryl maltoside neopentyl glycol (LMNG) supplemented with cholesteryl hemisuccinate (CHS) at 10:1 w/w ratio. Proteins were affinity purified in LMNG/CHS, and subsequently exchanged to digitonin by size exclusion chromatography.

The following are the list of constructs expressed and purified for this TEP.

Construct	Description
KCC1-Δ19	KCC1 with 19-residue deletion (M1 – N19) on the N-terminus for constitutive activation
KCC3b-WT	Wild-type full-length KCC3b
KCC3b-PM	Full-length KCC3b with phosphomimicking S45D/T940D/T991D mutations for inactivation
KCC3b-PKO	Full-length KCC3b with phospho-inhibited S45A/T940A/T991A mutations for constitutive activation

Structures

We determined the structure of KCC1-Δ19, KCC3b-WT and KCC3b-PM using cryo-electron microscopy (cryo-EM) to 3.1 Å, 3.7 Å and 3.2 Å resolutions respectively (**Fig. 2**).

KCC1 and KCC3 are 220 kDa homodimers consisting of two domains, the N-terminal transmembrane domain (TMD) and the cytoplasmic C-terminal domain (CTD), a typical architecture of CCC family. Their subunits form domain swapping at an alpha helix linking the TMD to CTD, hence forming a stable arrangement. The TMD is structurally a member of the amino acid polyamine organocation (APC) superfamily, where its twelve transmembrane helices are directly involved in the co-transport of potassium and chloride ions.

An important discovery from our KCC1 structure is the role of CTD, which is poorly understood. The CTD consists of two lobes, with the N-terminal lobe taking a classical Rossmann-like fold of alternating alpha helices and beta strands. In our structure, adenosine triphosphate (ATP) was discovered bound to this N-terminal lobe at a classical nucleotide binding site for Rossmann fold proteins (**Fig. 2A, 3**). Interestingly, both the location of the ATP and its binding mode are nearly identical to that of a *Halomonas elongata* stress-response protein TeaD (**Fig. 3C**), whose primary role is the regulation of TeaABC transporter (2). TeaABC transporter regulates the organism's cell volume via export of organic solutes, a function shared with KCC1 in red blood cells. This suggests a similar ATP-mediated regulation of KCC transporters via its CTD.

The ATP-binding pocket of KCC1 can be utilised for the design and development of KCC1 and KCC3-specific inhibitors. Proteins in the CCC family have different sets of amino acids lining this pocket, making it unique between them. In our structure, KCC3 does not feature ATP in its binding site despite being the closest member to KCC1 in the CCC family. The binding pocket for KCC3 is less accommodating to ATP due to larger side chain in the adenosine area (KCC1:V770 to KCC3:L784) as well as fewer hydrophilic interactions (KCC1:Y708 to KCC3:H722). The ATP-binding site for *Danio rerio* NKCC1 also has significant sequence differences to that of KCC1 (**fig 3B**). Therefore, this ATP binding pocket presents an opportunity to develop modulators specific to KCC1 or KCC3.

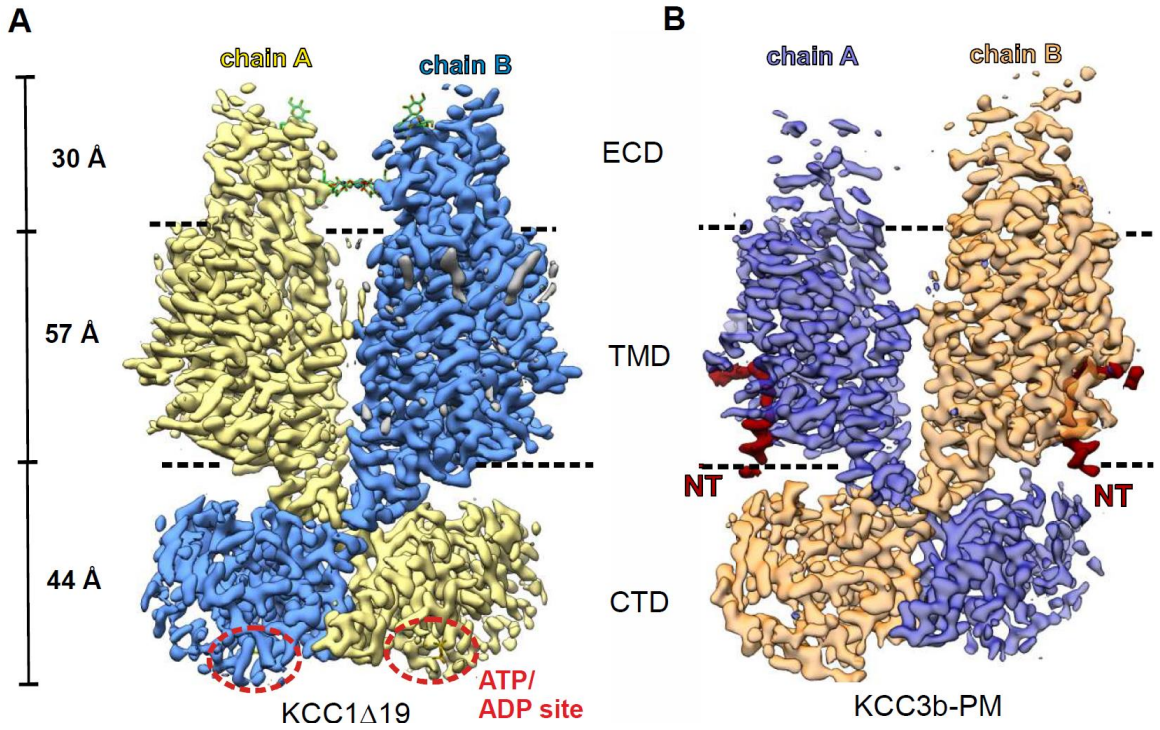

Figure 2. Cryo-EM structures of KCC1-Δ19 **(A)** and KCC3b-PM **(B)**. KCC1 and KCC3 show similar homodimeric architecture with domain swapping between transmembrane domain (TMD) and cytoplasmic C-terminal domain (CTD). KCC3b-PM features N-terminal plug (NT; red density) in the structure, and KCC1-Δ19 shows ATP binding in the CTD (red circle). ECD stands for extracellular domain, and the green molecules in KCC1 represent glycosylation. PDB ID: 6AIP (KCC1-Δ19), 6AIN (KCC3b-PM)

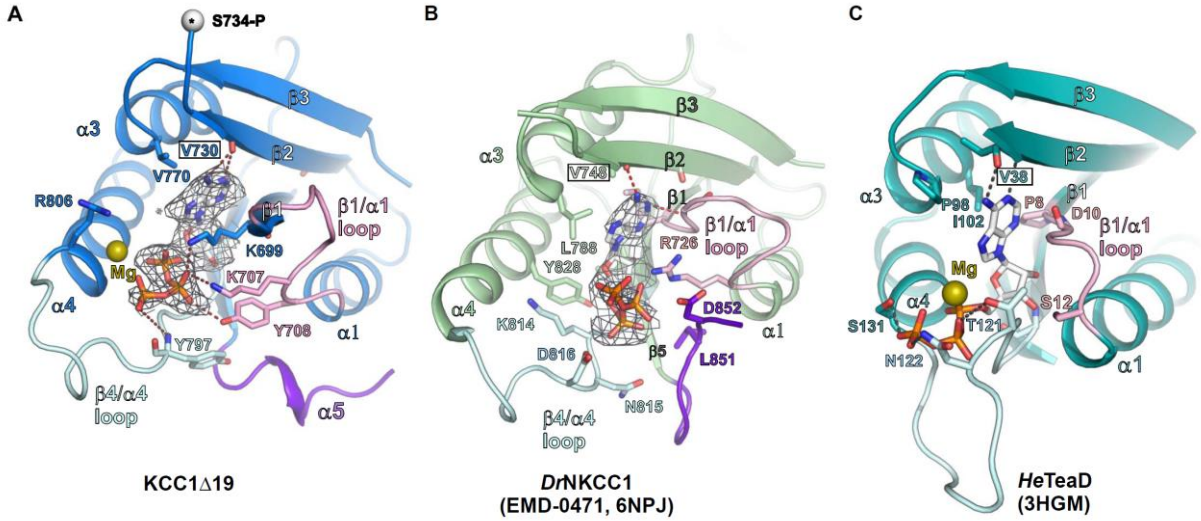

Figure 3. ATP-binding sites of KCC1-Δ19 (**A**), *Danio rerio* NKCC1 (**B**) (1), and *Halomonas elongata* TeaD (**C**) (2).

Compared to KCC1 structures, KCC3b-WT and KCC3b-PM show important differences on the cytoplasmic side of TMD, with potential functional implications. In KCC3b-PM, the 20-residue stretch of the N-terminus sits on the inorganic ion entry site (**Fig. 4A**), effectively blocking the transport of potassium and chloride ions. This N-terminal "plug" would also lock the TMD in the inward-facing state, which would prevent its transition between inward and outward-facing states for activity. On the other hand, the N-terminal plug is absent in the structure of KCC3b-WT (**Fig. 4B**), suggesting that it is at least partially in the active state. This observation is further supported by flexibility analysis of the two cryo-EM datasets: TMD subunits are largely rigid in KCC3b-PM, whereas transmembrane helices bend in inward and outward-like motions in the case of KCC3b-WT. The cytoplasmic pocket where the N-terminal plug sits is hence a potential site for the

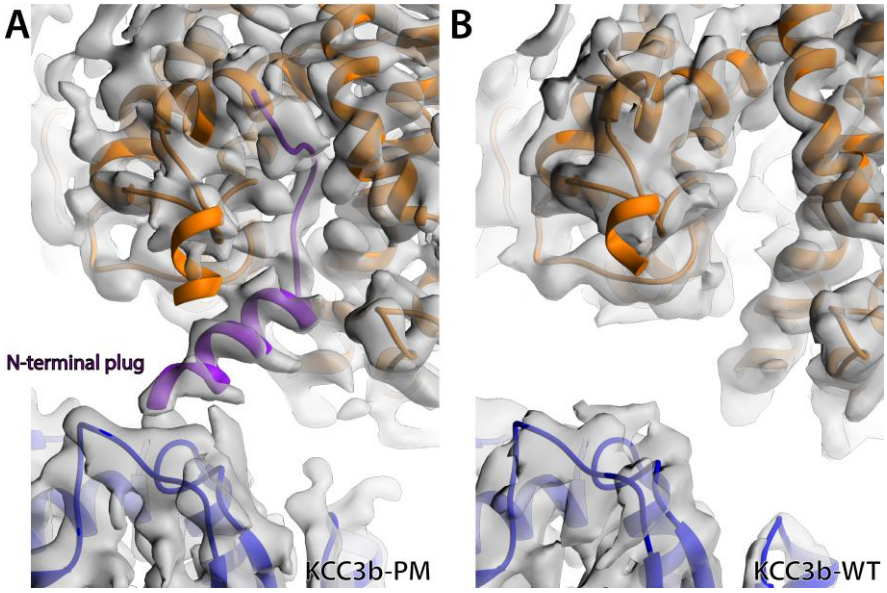

Figure 4. N-terminal plug site for KCC3. Orange – Transmembrane domain (TMD); Purple – N-terminal plug; Blue – C-terminal domain (CTD). In KCC3b-PM (**A**), which has mutations for reduced activity, the N-terminal strand occludes the pore entry. In wild-type KCC3b (**B**), however, this density is not present, leaving the pore open for K^+/Cl^- transport (empty pocket in the middle of TMD).

development of small molecule or peptide modulators, either preventing entry of the plug or blocking TMD transition between states depending on their structures.

Characterisation of chemical matters

We identified ATP binding to KCC1, but not KCC3, in the cryo-EM structures. We used a combination of thermal shift assay (TSA) (**Fig. 5A**), liquid chromatography/ mass spectrometry (LC-MS) and molecular dynamics (MD) experiment (**Fig. 5B**) to confirm the binding of adenosine nucleotides to KCC1 and KCC3. KCC1-Δ19 and KCC3b constructs have melting temperatures (T_m) of 45 – 50 °C in the apo state. ATP, adenosine diphosphate (ADP) and adenosine monophosphate (AMP) have been found to increase their thermostability by as high as 8 °C. On the other hand, guanosine triphosphate did not increase T_m significantly, indicating that KCC1 and KCC3 specifically bind to adenosine nucleotides. Adenosine nucleotides showed only weak binding to NKCC1, which belongs to a separate branch ($Na^+/K^+/Cl^-$ co-transporter) of the CCC family. KCC1 binding to these nucleotides was also confirmed with LC-MS where

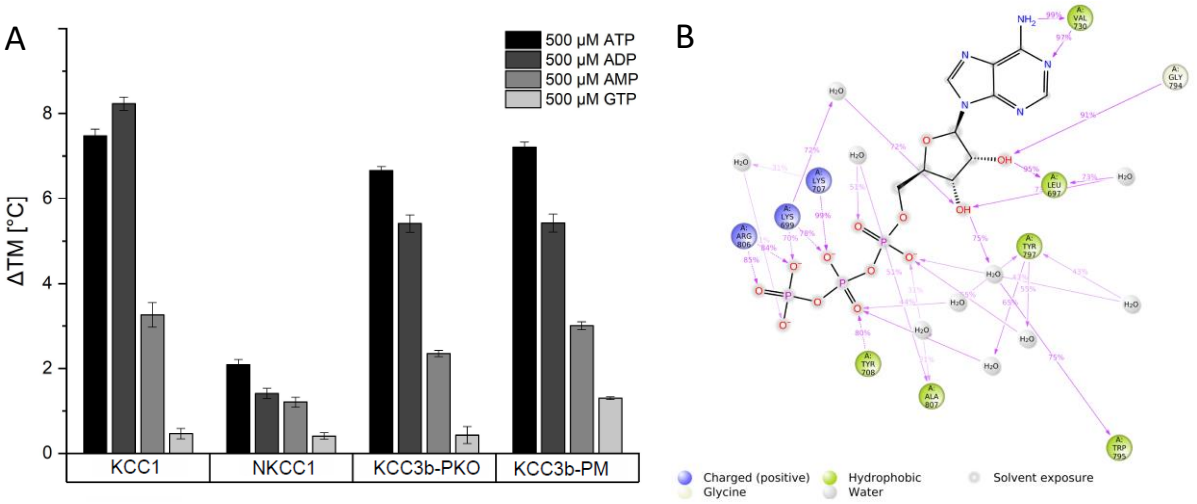

Figure 5. Thermal shift assays and molecular dynamics simulation of CCC transporters for studying ATP/ADP binding. (**A**) Thermal shift assay shows that ATP and ADP provide differing levels of thermostability to KCC1, NKCC1 and KCC3. Error bars indicate 95 % confidence level. (**B**) MD simulation of KCC1 shows well-coordinated interaction between the protein and ATP.

endogenous ADP and ATP from expressed cells were pulled down with KCC1 even after extensive washing steps of purification.

In order to probe if this ATP-binding pocket is a good candidate for a KCC1-specific modulator, we have performed MD simulations on both KCC1 and closely related KCC3 in collaboration with OMass Therapeutics (UK). Whereas ATP formed a number of interactions with KCC1 residues (**fig 5B**) and remained bound in the pocket throughout the 300 ns duration of the simulation, it formed far fewer interactions with KCC3 residues and drifted away from the binding site after ~150 ns. This result is consistent with observation from our cryo-EM data, where ATP is present only in KCC1 and not in KCC3. These experiments show that KCC1 has much slower rate of dissociation with ATP compared to KCC3, providing potential for the development of compounds specific to each member of the family.

Rubidium flux assays in oocytes

In collaboration with Paul Isenring's group at the University of Montréal (Canada), we performed oocyte assay to test if the N-terminal deletion of 19 residues made KCC1 constitutively active. In line with previous literature, full-length wild-type KCC1 is inactive in isotonic conditions (**Fig. 6A**), but shows high activity in hypotonic environment as measured in flux assay using rubidium as cargo. On the other hand, KCC1-Δ19 used in our cryo-EM studies was active in both isotonic and hypotonic conditions, providing experimental evidence that the structure represents an activated state.

We also performed this assay to study the effect of KCC3b mutations on the protein function (**Fig. 6B**). KCC3b-WT was activated only in hypotonic conditions, remaining inactive in isotonic environment. KCC3b-PKO, whose S45A/T940A/T991A mutations knock out inactivating phosphorylations (i.e. keeping KCC3 constitutively active) showed very high levels of activity regardless of osmotic gradient. On the other hand, KCC3b-PM, whose S45D/T940D/T991D mutations mimic inactivating phosphorylations, showed low level of activity independent of osmotic gradient. These results confirm KCC3b-PM as an inactive or less-active form of the protein.

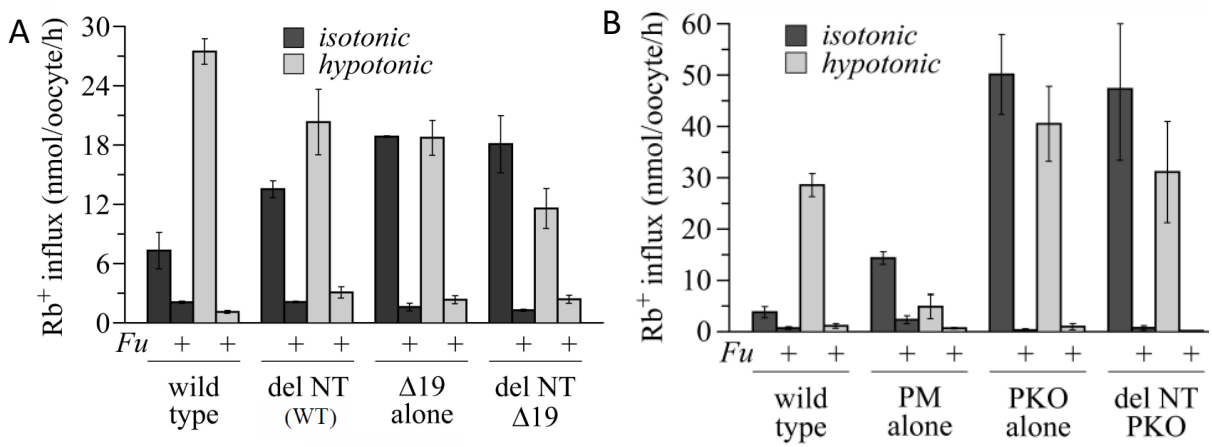

Figure 6. Rubidium flux assays of KCC1 and KCC3b constructs. (A) Wild-type constructs of both KCC1 and KCC3 are inactive in isotonic conditions, and become active in hypotonic environment. Both partial N-terminal deletion covering the first 19 residues (Δ19) and full deletions including the N-terminal plug (del NT) make the transporter constitutively active. (B) KCC3b-PM becomes insensitive to cell osmolarity due to mutations at the phosphorylation site and shows reduced activity compared to both wild-type and constitutively-active KCC3b-PKO mutant.

Phosphoproteomics mass spectrometry of KCC1

We mapped phosphorylation sites of KCC1 using MS/MS in collaboration with Carol Robinson's group (Oxford) to understand phosphoregulation of KCC1, a key modification by which its activity is controlled. We found that serine-88 of KCC1-Δ19 is not phosphorylated, providing further support for this construct being in active state. In the process, we found this construct to be phosphorylated at four other sites instead, two

of which have not been described in the previous literature. One of them, S916, is located at the hinge point where α8 helix of CTD shows considerable flexibility, suggesting its role in KCC1 regulation.

IMPORTANT: Please note that the existence of small molecules within this TEP indicates only that chemical matter might bind to the protein in potentially functionally relevant locations. The small molecule ligands are intended to be used as the basis for future chemistry optimisation to increase potency and selectivity and yield a chemical probe or lead series. As such, the molecules within this TEP should not be used as tools for functional studies of the protein, unless otherwise stated, as they are not sufficiently potent or well-characterised to be used in cellular studies.

CONCLUSION

Biological understanding

We have determined high-resolution cryo-EM structures of human KCC1 and KCC3 in their dimeric states including CTD. The KCC1 structure shows a novel ATP-binding site in the CTD, whose location and binding mode suggests an adenosine nucleotide and Mg^{2+}-mediated regulation of KCC transporters. ATP has tighter binding to KCC1 compared to KCC3 and NKCC1 in MD simulation and thermal shift assays, suggesting that members of the CCC family have different affinities to it. New phosphorylation sites mapped for KCC1 and KCC3 may have accessory roles in the regulation of their function.

Medical relevance

Structures of KCC1 and KCC3 reveal several potential compound-binding pockets, enabling *in silico* drug designs specific to it for the treatment of sickle cell diseases (SCD), β-thalassaemia and genetic neurological disorders.

Understanding of regulatory mechanisms behind KCC1 activity will help with understanding the pathogenesis of SCD including cell dehydration and positive feedback cycle.

Disease mutants of KCC3 can be mapped on its structure, which will assist medical researchers and practitioners with improved identification of patients and treatment strategies.

Ongoing and Future plans

The biophysical assays and structural data obtained from this project are taken forward in the new EUbOPEN and ReSOLUTE programs from the unit, to discover both new biological entities and chemical entities targeting each of the KCC transporters. We plan to screen small molecule modulators of KCC1 as part of the IMI-funded EUbOPEN project focused on the probe development. KCC3 will be used as negative selectors to ensure that we identify compounds which are selective to KCC1 only. Both full-length and CTD-only constructs of KCC1 and KCC3 can be purified to identify if the newly identified compounds bind to CTD or TMD. Additionally KCC3 is part of the ongoing ReSOLUTE program to generate binders for the protein, and to set up cellular and in vitro assays. To this end, KCC3-specific sybodies have been generated recently in collaboration with Dr. Eric Geertsma as part of this program. Three of the sybodies have been characterised and shown to bind to the N-terminal end of KCC3, with one binding tightly enough for co-purification. We next plan to perform epitope mapping of KCC3 using structural biology techniques, primarily cryo-EM.

TEP IMPACT

Publications arising from this work:

This work has been submitted for review in a journal.

FUNDING INFORMATION

The work performed at the SGC has been funded by a grant from the Innovative Medicines Initiative Joint Undertaking ULTRA-DD grant 115766 and the Wellcome Trust 106169/ZZ14/Z.

ADDITIONAL INFORMATION

Structure Files

PDB ID	Structure Details
7AIP	Structure of human KCC1 in complex with ATP (reference map/model)
7AIQ	Structure of human KCC1 in complex with ATP (subclass 1)
7AIR	Structure of human KCC1 in complex with ATP (subclass 2)
7AIN	Structure of human KCC3b-PM in NaCl
7AIO	Structure of human KCC3b-PM in NaCl (subclass)
6Y5V	Structure of human KCC3b-PM in KCl

Materials and Methods

Molecular biology, virus production and protein expression

Full-length and Δ19-deleted human KCC1 (isoform A) and KCC3 isoform B were cloned from the mammalian gene collection (MGC: 1455 and 161519, IMAGE ID: 3349710 and 8991957, respectively) into LIC-adapted pHTBV C-terminally tagged twin-strep, 10-His vector with and without GFP. Full-length NKCC1, KCC2, and phospho-mimetic (S45D, T940D, T997D) and phospho-knockout (S45A, T940A, T997A) constructs of KCC3b were synthesised (GenScript, Twist Bioscience) and subcloned into LIC-adapted pHTBV C-terminally tagged twin-strep, 10-His vector with GFP.

Below are the DNA sequences of the constructs used in this study.

KCC1-Δ19

MPHFTVVPVDGPRRGDYDNLEGLSWVDYGERAELDDSDGHGNHRESSPFLSPLEASRGIDYYDRNLALFEEELDIRPKVS
SLLGKLVSYTNLTQGAKEHEEAESGEGTRRRAAEAPSMGTLMGVYLPCLQNIFGVILFLRLTWMVGTAGVLQALLIVLICC
CCTLLTAISMSAIATNGVVPAGGSYFMISRSLGPEFGGAVGLCFYLGTTFAAAMYILGAIEILLTYIAPPAAIFYPSGAHDTSN
ATLNNMRVYGTIFLTFMTLVVFVGVKYVNKFASLFLACVIISILSIYAGGIKSIFDPPVFPVCMLGNRTLSRDQFDICAKTAVV
DNETVATQLWSFFCHSPNLTTDSCDPYFMLNNVTEIPGIPGAAAGVLQENLWSAYLEKGDIVEKHGLPSADAPSLKESLPL
YVVADIATSFTVLVGIFFPSVTGIMAGSNRSGDLRDAQKSIPVGTILAIITTSLVYFSSVVLFGACIEGVVLRDKYGDGVSRNL
VVGTLAWPSPWVIVIGSFFSTCGAGLQSLTGAPRLLQAIAKDNIIPFLRVFGHGKVNGEPTWALLLTALIAELGILIASLDMV
APILSMFFLMCYLFVNLACAVQTLLRTPNWRPRFKYYHWALSFLGMSLCLALMFVSSWYYALVAMLIAGMIYKYIEYQGA
EKEWGDGIRGLSLSAARYALLRLEEGPPHTKNWRPQLLVLLKLDEDLHVKYPRLLTFASQLKAGKGLTIVGSVIQGSFLESYG
EAQAAEQTIKNMMEIEKVKGFCQVVVASKVREGLAHLIQSCGLGGMRHNSVVLGWPYGWRQSEDPRAWKTFIDTVRC
TTAAHLALLVPKNIAFYPSNHERYLEGHIDVWWIVHDGGMLMLLPFLLRQHKVWRKCRMRIFTVAQMDDNSIQMKKDL
AVFLYHLRLEAEVEVVEMHNSDISAYTYERTLMMEQRSQMLRQMRLTKTERENEAQLVKDRHSALRLESLYSDEEDESAV
GADKIQMTWTRDKYMTETWDPSHAPDNFRELVHIKPDQSNVRRMHTAVKLNEVIVTRSHDARLVLLNMPGPPRNSEG
DENYMEFLEVLTEGLERVLLVRGGGREV

KCC3b-WT

MPHFTVTKVEDPEEGAAASISQEPSLADIKARIQDSDEPDLSQNSITGEHSQLLDDGHKKARNAYLNNSNYEEGDEYFDK
NLALFEEEMDTRPKVSSLLNRMANYTNLTQGAKEHEEAENITEGKKKPTKTPQMGTFMGVYLPCLQNIFGVILFLRLTWV
VGTAGVLQAFAIVLICCCCTMLTAISMSAIATNGVVPAGGSYFMISRALGPEFGGAVGLCFYLGTTFAAAMYILGAIEIFLVY
IVPRAAIFHSDDALKESAAMLNNMRVYGTAFLVLMVLVVFIGVRYVNKFASLFLACVIVSILAIYAGAIKSSFAPPHFPVCML
GNRTLSSRHIDVCSKTKEINNMTVPSKLWGFFCNSSQFFNATCDEYFVHNNVTSIQGIPGLASGIITENLWSNYLPKGEIIEK
PSAKSSDVLGSLNHEYVLVDITTSFTLLVGIFFPSVTGIMAGSNRSGDLKDAQKSIPIGTILAILTTSFVYLSNVVLFGACIEGVV
LRDKFGDAVKGNLVVGTLSWPSPWVIVIGSFFSTCGAGLQSLTGAPRLLQAIAKDNIIPFLRVFGHSKANGEPTWALLLTA
AIAELGILIASLDLVAPILSMFFLMCYLFVNLACALQTLLRTPNWRPRFRYYHWALSFMGMSICLALMFISSWYYAIVAMVI
AGMIYKYIEYQGAEKEWGDGIRGLSLSAARFALLRLEEGPPHTKNWRPQLLVLLKLDEDLHVKHPRLLTFASQLKAGKGLTI
VGSVIVGNFLENYGEALAAEQTIKHLMEAEKVKGFCQLVVAAKLREGISHLIQSCGLGGMKHNTVVMGWPNGWRQSED
ARAWKTFIGTVRVTTAAHLALLVAKNISFFPSNVEQFSEGNIDVWWIVHDGGMLMLLPFLLKQHKVWRKCSIRIFTVAQL

EDNSIQMKKDLATFLYHLRIEAEVEVVEMHDSDISAYTYERTLMMEQRSQMLRHMRLSKTERDREAQLVKDRNSMLRLT
SIGSDEDEETETYQEKVHMTWTKDKYMASRGQKAKSMEGFQDLLNMRPDQSNVRRMHTAVKLNEVIVNKSHEAKLVL
LNMPGPPRNPEGDENYMEFLEVLTEGLERVLLVRGGGSEVITIYS

KCC3b-PM

MPHFTVTKVEDPEEGAAASISQEPSLADIKARIQDSDEPDLSQNDITGEHSQLLDDGHKKARNAYLNNSNYEEGDEYFDK
NLALFEEEMDTRPKVSSLLNRMANYTNLTQGAKEHEEAENITEGKKKPTKTPQMGTFMGVYLPCLQNIFGVILFLRLTWV
VGTAGVLQAFAIVLICCCCTMLTAISMSAIATNGVVPAGGSYFMISRALGPEFGGAVGLCFYLGTTFAAAMYILGAIEIFLVY
IVPRAAIFHSDDALKESAAMLNNMRVYGTAFLVLMVLVVFIGVRYVNKFASLFLACVIVSILAIYAGAIKSSFAPPHFPVCML
GNRTLSSRHIDVCSKTKEINNMTVPSKLWGFFCNSSQFFNATCDEYFVHNNVTSIQGIPGLASGIITENLWSNYLPKGEIIEK
PSAKSSDVLGSLNHEYVLVDITTSFTLLVGIFFPSVTGIMAGSNRSGDLKDAQKSIPIGTILAILTTSFVYLSNVVLFGACIEGVV
LRDKFGDAVKGNLVVGTLSWPSPWVIVIGSFFSTCGAGLQSLTGAPRLLQAIAKDNIIPFLRVFGHSKANGEPTWALLLTA
AIAELGILIASLDLVAPILSMFFLMCYLFVNLACALQTLLRTPNWRPRFRYYHWALSFMGMSICLALMFISSWYYAIVAMVI
AGMIYKYIEYQGAEKEWGDGIRGLSLSAARFALLRLEEGPPHTKNWRPQLLVLLKLDEDLHVKHPRLLTFASQLKAGKGLTI
VGSVIVGNFLENYGEALAAEQTIKHLMEAEKVKGFCQLVVAAKLREGISHLIQSCGLGGMKHNTVVMGWPNGWRQSED
ARAWKTFIGTVRVTTAAHLALLVAKNISFFPSNVEQFSEGNIDVWWIVHDGGMLMLLPFLLKQHKVWRKCSIRIFTVAQL
EDNSIQMKKDLATFLYHLRIEAEVEVVEMHDSDISAYTYERDLMMEQRSQMLRHMRLSKTERDREAQLVKDRNSMLRLT
SIGSDEDEETETYQEKVHMDWTKDKYMASRGQKAKSMEGFQDLLNMRPDQSNVRRMHTAVKLNEVIVNKSHEAKLVL
LNMPGPPRNPEGDENYMEFLEVLTEGLERVLLVRGGGSEVITIYS

KCC3b-PKO

MPHFTVTKVEDPEEGAAASISQEPSLADIKARIQDSDEPDLSQNAITGEHSQLLDDGHKKARNAYLNNSNYEEGDEYFDK
NLALFEEEMDTRPKVSSLLNRMANYTNLTQGAKEHEEAENITEGKKKPTKTPQMGTFMGVYLPCLQNIFGVILFLRLTWV
VGTAGVLQAFAIVLICCCCTMLTAISMSAIATNGVVPAGGSYFMISRALGPEFGGAVGLCFYLGTTFAAAMYILGAIEIFLVY
IVPRAAIFHSDDALKESAAMLNNMRVYGTAFLVLMVLVVFIGVRYVNKFASLFLACVIVSILAIYAGAIKSSFAPPHFPVCML
GNRTLSSRHIDVCSKTKEINNMTVPSKLWGFFCNSSQFFNATCDEYFVHNNVTSIQGIPGLASGIITENLWSNYLPKGEIIEK
PSAKSSDVLGSLNHEYVLVDITTSFTLLVGIFFPSVTGIMAGSNRSGDLKDAQKSIPIGTILAILTTSFVYLSNVVLFGACIEGVV
LRDKFGDAVKGNLVVGTLSWPSPWVIVIGSFFSTCGAGLQSLTGAPRLLQAIAKDNIIPFLRVFGHSKANGEPTWALLLTA
AIAELGILIASLDLVAPILSMFFLMCYLFVNLACALQTLLRTPNWRPRFRYYHWALSFMGMSICLALMFISSWYYAIVAMVI
AGMIYKYIEYQGAEKEWGDGIRGLSLSAARFALLRLEEGPPHTKNWRPQLLVLLKLDEDLHVKHPRLLTFASQLKAGKGLTI
VGSVIVGNFLENYGEALAAEQTIKHLMEAEKVKGFCQLVVAAKLREGISHLIQSCGLGGMKHNTVVMGWPNGWRQSED
ARAWKTFIGTVRVTTAAHLALLVAKNISFFPSNVEQFSEGNIDVWWIVHDGGMLMLLPFLLKQHKVWRKCSIRIFTVAQL
EDNSIQMKKDLATFLYHLRIEAEVEVVEMHDSDISAYTYERALMMEQRSQMLRHMRLSKTERDREAQLVKDRNSMLRLT
SIGSDEDEETETYQEKVHMAWTKDKYMASRGQKAKSMEGFQDLLNMRPDQSNVRRMHTAVKLNEVIVNKSHEAKLVL
LNMPGPPRNPEGDENYMEFLEVLTEGLERVLLVRGGGSEVITIYS

NKCC1

MEPRPTAPSSGAPGLAGVGETPSAAALAAARVELPGTAVPSVPEDAAPASRDGGGVRDEGPAAAGDGLGRPLGPTPSQ
SRFQVDLVSENAGRAAAAAAAAAAAAAAAGAGAGAKQTPADGEASGESEPAKGSEEAKGRFRVNFVDPAASSSAEDSL
SDAAGVGVDGPNVSFQNGGDTVLSEGSSLHSGGGGGSGHHQHYYYDTHTNTYYLRTFGHNTMDAVPRIDHYRHTAAQ
LGEKLLRPSLAELHDELEKEPFEDGFANGEESTPTRDAVVTYTAESKGVVKFGWIKGVLVRCMLNIWGVMLFIRLSWIVGQ
AGIGLSVLVIMMATVVTTITGLSTSAIATNGFVRGGGAYYLISRSLGPEFGGAIGLIFAFANAVAVAMYVVGFAETVVELLKE
HSILMIDEINDIRIIGAITVVILLGISVAGMEWEAKAQIVLLVILLLAIGDFVIGTFIPLESKKPKGFFGYKSEIFNENFGPDFREE
ETFFSVFAIFFPAATGILAGANISGDLADPQSAIPKGTLLAILITTLVYVGIAVSVGSCVVRDATGNVNDTIVTELTNCTSAACK
LNFDFSSCESSPCSYGLMNNFQVMSMVSGFTPLISAGIFSATLSSALASLVSAPKIFQALCKDNIYPAFQMFAKGYGKNNE
PLRGYILTFLIALGFILIAELNVIAPIISNFFLASYALINFSVFHASLAKSPGWRPAFKYYNMWISLLGAILCCIVMFVINWWAA
LLTYVIVLGLYIYVTYKKPDVNWGSSTQALTYLNALQHSIRLSGVEDHVKNFRPQCLVMTGAPNSRPALLHLVHDFTKNVG
LMICGHVHMGPRRQAMKEMSIDQAKYQRWLIKNKMKAFYAPVHADDLREGAQYLMQAAGLGRMKPNTLVLGFKKD
WLQADMRDVDMYINLFHDAFDIQYGVVVIRLKEGLDISHLQGQEELLSSQEKSPGTKDVVVSVEYSKKSDLDTSKPLSEKP
ITHKVEEEDGKTATQPLLKKESKGPIVPLNVADQKLLEASTQFQKKQGKNTIDVWWLFDDGGLTLLIPYLLTTKKKWKDCKI
RVFIGGKINRIDHDRRAMATLLSKFRIDFSDIMVLGDINTKPKKENIIAFEEIIEPYRLHEDDKEQDIADKMKEDEPWRITDN
ELELYKTKTYRQIRLNELLKEHSSTANIIVMSLPVARKGAVSSALYMAWLEALSKDLPPILLVRGNHQSVLTFYS

Baculoviral DNA from the transformation of DH10Bac were used to transfect Sf9 cells to produce baculovirus particles for transduction. Virus was amplified by transducing mid-log Sf9 cells (2×10^6 cells mL^{-1}) grown in Sf-900™ II media supplemented with 2 % fetal bovine serum (Thermo Fisher Scientific). Cells were incubated on an orbital shaker for 65 h at 27 °C in 1 L shaker flasks. Baculovirus were harvested by centrifugation at 900*g* for 10 min with the virus contained in the supernatant.

1 L of Expi293F™ GnTI- cell cultures (2×10^6 cells mL^{-1}) in Freestyle 293™ Expression Medium (Thermo Fisher Scientific) were infected with high-titre P3 baculovirus (3 % v/v) in the presence of 5 mM sodium butyrate in a 2 L roller bottle (Biofil). Cells were grown in a humidity-controlled orbital shaker for 48 h at 37 °C with 8 % CO2 before being harvested by centrifugation at 900*g* for 10 min, washed with phosphate-buffered saline, and pelleted again prior to flash freezing in liquid nitrogen (LN2), then stored at −80 °C until needed.

Protein purification of digitonin samples

Whole cell pellets expressing varying constructs of NKCC1, KCC1, KCC2 and KCC3b were resuspended to a total volume of 50 mL per 15 g of cell pellet with buffer A (150 mM NaCl, 20 mM HEPES pH 7.5) supplemented with, 0.7 % w/v Lauryl Maltose Neopentyl Glycol, LMNG (Generon), and 0.07 % cholesteryl hemisuccinate, CHS (Generon). The cells were solubilised at 4 °C for 1 h with gentle rotation. Cell debris was pelleted at 50,000*g* for 30 min. The clarified lysate was added to 0.5 mL bed volume of Strep-Tactin SuperFlow (IBA) per 50 mL of lysate, and allowed to bind at 4 °C for 1 h. The resin was collected on a gravity-flow column and washed with buffer B (buffer A with 0.003 % w/v LMNG and 0.0003 % w/v CHS), and then with buffer B supplemented with 1 mM ATP and 5 mM $MgCl_2$. Protein was eluted with 7 CV of buffer B supplemented with 5 mM D-desthiobiotin followed by tag-cleavage by TEV protease overnight and reverse purification. For LMNG/CHS condition, the samples were subjected to size exclusion chromatography pre-equilibrated with Buffer B. For digitonin condition, buffer A supplemented with 0.04 % digitonin (Apollo Scientific) was used for equilibration instead. Peak fractions were pooled and concentrated to 5 µM for LMNG/CHS sample and 50 µM for digitonin sample for subsequent experiments.

Nanodisc sample was prepared similarly to the detergent samples with a few exceptions. After washing the protein-bound Strep-Tactin resin, buffer A supplemented with 0.5 % LMNG, 0.05% CHS and 0.125 % soy azolectin (Sigma) was added to a final LMNG concentration of 0.2 %, and purified MSP E3D1 protein to a final concentration of 0.5 mg/mL. The slurry was incubated on a rotating wheel for 15 min, then 100 mg of washed Biobead SM-2 per mL resin was added, followed by further incubation for a minimum of 4 hours. Subsequent purifications were then performed with buffer A.

Cryo-electron microscopy sample preparation, data collection and data processing

All samples were frozen on Quantifoil Au R1.2/1.3 mesh 300 grids freshly glow discharged for 30 s, with plunge freezing performed on Vitrobot Mark IV (Thermo Fisher Scientific) chamber set to 80-100 % humidity and 4 °C. For LMNG/CHS and MSP E3D1 conditions, blotting time was set to 1.0 – 1.5 s, and for digitonin conditions it was set to 3.5 – 5.0 s after 30 s wait time.

The cryo-EM datasets were collected on Titan Krioses (Thermo Fisher Scientific) operating at 300 keV. Super-resolution dose-fractionated micrographs (0.3255 Å $pixel^{-1}$ or 0.415 Å $pixel^{-1}$) were collected on a K3 (Gatan) detector by image shift collection two exposures per hole with a total dose of 40 – 45 $e^- Å^{-2}$. Micrographs were binned 2 x 2 during motion correction with 5 by 5 patches using MotionCor2. Motion-corrected images were then processed in Cryosparc 2.11.0 where defocus values were determined by Patch CTF function on Cryosparc. Particles were picked with blob picker function, and extracted particles were subjected to two cycles of 2D classification. Particles from good classes were used to generate three ab-initio models. Particles in the good model class were then used for non-uniform refinement function with C2 symmetry using the ab-initio model as reference.

Rb^+ flux assays

Defolliculated stage V–VI *Xenopus laevis* oocytes were microinjected with KCC-derived cRNAs (same amount between WT and mutants for each of the KCC1 and KCC3b isoforms) and maintained in Barth medium for 3 d at 18 °C in the presence of 1.5 mM furosemide. Water-injected oocytes were used as controls. Before the transport assay, furosemide was removed through several washes in plain Barth medium. Carrier activity was assessed at room temperature through Rb^+ influx assays under isotonic and hypotonic conditions. The experiments were carried out more specifically by incubating oocytes for 1 h in a hypotonic solution (125 mOsM) or in an isotonic solution (200 mOsM) and reincubating them afterwards for 45 min in an isotonic salt-added physiological solution (7 mM Rb^+, 86 mM Cl^-) in the presence or absence of 1.5 mM furosemide. At the end of flux assays, oocytes were washed several times in a refrigerated Rb^+-free solution, lysed in pure nitric acid and assayed for Rb^+ content (1 oocyte/sample) by atomic absorption spectrophotometry (Varian AA240). Transport data for oocytes are expressed in this work as mean (± S.E.) background-subtracted transport rates in 10 oocytes among 3 to 6 experiments.

LC-MS analysis for small molecule identification

The purified KCC1 protein sample was initially buffer exchange into 200 mM ammonium acetate at pH 7.4 using a bipspin column (Bio-rad) and resuspended in 100 µL of water with 0.1 % formic acid to be analyzed by LC-MS/MS. The separation was performed using an Ascentis Express C18 analytical column (0.3 x 150 mm, 2.7 µm) at 15 µL.min-1 using the isocratic elution with following mobile phases, A – water with 0.1 % formic acid and B – acetonitrile with 0.1 % formic acid at 97:3 (v/v), respectively. The sample volume injected was 1 µL and the total run time was 3 min. All measurements were performed using the Orbitrap Eclipse Tribrid mass spectrometer coupled with Ultimate 3000 binary pump. The MS was operated in negative polarity and the ionization conditions were 275 °C for capillary temperature (ion transfer tube), 20 °C for vaporizer temperature and 3500 V for spray voltage. Thermo Xcalibur software was used for data processing.

NanoDSF measurements

All KCC variants were diluted up to 0.2 mg/ml in protein buffer (20 mM HEPES pH 7.4, 150 mM NaCl, digitonin). 10 x nucleotide stock solutions in were prepared in protein buffer. Protein and nucleotides were mixed and incubated on ice for 30 min. NT.Plex nanoDSF Grade High Sensitivity Capillaries (NanoTemper) were filled with 10-µl protein sample. Melting curves were determined in triplicates using Prometheus NT.48 by monitoring the intrinsic protein fluorescence signal as a measure of its folding state during a temperature ramp (1 °C/min increase) from 20 to 95°C. Exemplary melting curves are shown in Supplementary Figure 3. The melting temperature was determined by averaging the melting temperature of the triplicate measurements.

Molecular Dynamics Simulations

The MD simulations were carried out using Desmond simulation package of Schrödinger LLC. The NPT ensemble with the temperature 300 K and a pressure 1 bar was applied in all runs. The simulation length was 500 ns with a relaxation time 1 ps for the ligand ATP. The OPLS3e force field parameters were used in all simulations. The long-range electrostatic interactions were calculated using the particle mesh Ewald method. The cutoff radius in Coulomb interactions was 9.0 Å. The water molecules were explicitly described using the simple point charge model. The Martyna–Tuckerman–Klein chain coupling scheme with a coupling constant of 2.0 ps was used for the pressure control and the Nosé–Hoover chain coupling scheme for the temperature control. Non-bonded forces were calculated using an r-RESPA integrator where the short-range forces were updated every step and the long-range forces were updated every three steps. The trajectories were saved at 200 ps intervals for analysis. The behaviour and interactions between the ligands and protein were analysed

using the Simulation Interaction Diagram tool implemented in Desmond MD package. The stability of MD simulations was monitored by looking on the rmsd of the ligand and protein atom positions in time.

References

We respectfully request that this document is cited using the DOI value as given above if the content is used in your work.

1. Chew, T. A., Orlando, B. J., Zhang, J., Latorraca, N. R., Wang, A., Hollingsworth, S. A., Chen, D.-H., Dror, R. O., Liao, M., and Feng, L. (2019) Structure and mechanism of the cation–chloride cotransporter NKCC1. *Nature* **572**, 488-492
2. Schweikhard, E. S., Kuhlmann, S. I., Kunte, H. J., Grammann, K., and Ziegler, C. M. (2010) Structure and function of the universal stress protein TeaD and its role in regulating the ectoine transporter TeaABC of Halomonas elongata DSM 2581(T). *Biochemistry* **49**, 2194-2204
3. Huang, H., Song, S., Banerjee, S., Jiang, T., Zhang, J., Kahle, K. T., Sun, D., and Zhang, Z. (2019) The WNK-SPAK/OSR1 Kinases and the Cation-Chloride Cotransporters as Therapeutic Targets for Neurological Diseases. *Aging Dis* **10**, 626-636
4. Kahle, K. T., Khanna, A. R., Alper, S. L., Adragna, N. C., Lauf, P. K., Sun, D., and Delpire, E. (2015) K-Cl cotransporters, cell volume homeostasis, and neurological disease. *Trends in molecular medicine* **21**, 513-523
5. Al Shibli, N., Al-Maawali, A., Elmanzalawy, A., Al-Nabhani, M., Koul, R., Gabr, A., and Al Murshedi, F. (2020) A Novel Splice-Site Variant in SLC12A6 Causes Andermann Syndrome without Agenesis of the Corpus Callosum. *Journal of pediatric genetics* **9**, 293-295
6. Bowerman, M., Salsac, C., Bernard, V., Soulard, C., Dionne, A., Coque, E., Benlefki, S., Hince, P., Dion, P. A., Butler-Browne, G., Camu, W., Bouchard, J. P., Delpire, E., Rouleau, G. A., Raoul, C., and Scamps, F. (2017) KCC3 loss-of-function contributes to Andermann syndrome by inducing activity-dependent neuromuscular junction defects. *Neurobiology of disease* **106**, 35-48
7. Crable, S. C., Hammond, S. M., Papes, R., Rettig, R. K., Zhou, G. P., Gallagher, P. G., Joiner, C. H., and Anderson, K. P. (2005) Multiple isoforms of the KC1 cotransporter are expressed in sickle and normal erythroid cells. *Experimental hematology* **33**, 624-631
8. Pan, D., Kalfa, T. A., Wang, D., Risinger, M., Crable, S., Ottlinger, A., Chandra, S., Mount, D. B., Hübner, C. A., Franco, R. S., and Joiner, C. H. (2011) K-Cl cotransporter gene expression during human and murine erythroid differentiation. *The Journal of biological chemistry* **286**, 30492-30503
9. Vitoux, D., Olivieri, O., Garay, R. P., Cragoe, E. J., Jr., Galacteros, F., and Beuzard, Y. (1989) Inhibition of K+ efflux and dehydration of sickle cells by [(dihydroindenyl)oxy]alkanoic acid: an inhibitor of the K+ Cl- cotransport system. *Proceedings of the National Academy of Sciences of the United States of America* **86**, 4273-4276
10. Brown, F. C., Conway, A. J., Cerruti, L., Collinge, J. E., McLean, C., Wiley, J. S., Kile, B. T., Jane, S. M., and Curtis, D. J. (2015) Activation of the erythroid K-Cl cotransporter Kcc1 enhances sickle cell disease pathology in a humanized mouse model. *Blood* **126**, 2863-2870
11. Rust, M. B., Alper, S. L., Rudhard, Y., Shmukler, B. E., Vicente, R., Brugnara, C., Trudel, M., Jentsch, T. J., and Hübner, C. A. (2007) Disruption of erythroid K-Cl cotransporters alters erythrocyte volume and partially rescues erythrocyte dehydration in SAD mice. *The Journal of clinical investigation* **117**, 1708-1717
12. Shmukler, B. E., Rivera, A., Bhargava, P., Nishimura, K., Kim, E. H., Hsu, A., Wohlgemuth, J. G., Morton, J., Snyder, L. M., De Franceschi, L., Rust, M. B., Hubner, C. A., Brugnara, C., and Alper, S. L. (2020) Genetic disruption of KCC cotransporters in a mouse model of thalassemia intermedia. *Blood cells, molecules & diseases* **81**, 102389
13. Delpire, E., and Weaver, C. D. (2016) Challenges of Finding Novel Drugs Targeting the K-Cl Cotransporter. *ACS chemical neuroscience* **7**, 1624-1627

14. Garay, R. P., Nazaret, C., Hannaert, P. A., and Cragoe, E. J., Jr. (1988) Demonstration of a [K+,Cl-]-cotransport system in human red cells by its sensitivity to [(dihydroindenyl)oxy]alkanoic acids: regulation of cell swelling and distinction from the bumetanide-sensitive [Na+,K+,Cl-]-cotransport system. *Molecular pharmacology* **33**, 696-701
15. Delpire, E., Baranczak, A., Waterson, A. G., Kim, K., Kett, N., Morrison, R. D., Daniels, J. S., Weaver, C. D., and Lindsley, C. W. (2012) Further optimization of the K-Cl cotransporter KCC2 antagonist ML077: development of a highly selective and more potent in vitro probe. *Bioorganic & medicinal chemistry letters* **22**, 4532-4535
16. Prael, F. J., 3rd, Chen, R., Li, Z., Reed, C. W., Lindsley, C. W., Weaver, C. D., and Swale, D. R. (2018) Use of chemical probes to explore the toxicological potential of the K(+)/Cl(-) cotransporter (KCC) as a novel insecticide target to control the primary vector of dengue and Zika virus, Aedes aegypti. *Pesticide biochemistry and physiology* **151**, 10-17
17. Mero, M., Asraf, H., Sekler, I., Taylor, K. M., and Hershfinkel, M. (2019) ZnR/GPR39 upregulation of K(+)/Cl(-)-cotransporter 3 in tamoxifen resistant breast cancer cells. *Cell calcium* **81**, 12-20